



저작자표시-비영리-변경금지 2.0 대한민국

이용자는 아래의 조건을 따르는 경우에 한하여 자유롭게

- 이 저작물을 복제, 배포, 전송, 전시, 공연 및 방송할 수 있습니다.

다음과 같은 조건을 따라야 합니다:



저작자표시. 귀하는 원저작자를 표시하여야 합니다.



비영리. 귀하는 이 저작물을 영리 목적으로 이용할 수 없습니다.



변경금지. 귀하는 이 저작물을 개작, 변형 또는 가공할 수 없습니다.

- 귀하는, 이 저작물의 재이용이나 배포의 경우, 이 저작물에 적용된 이용허락조건을 명확하게 나타내어야 합니다.
- 저작권자로부터 별도의 허가를 받으면 이러한 조건들은 적용되지 않습니다.

저작권법에 따른 이용자의 권리는 위의 내용에 의하여 영향을 받지 않습니다.

이것은 [이용허락규약\(Legal Code\)](#)을 이해하기 쉽게 요약한 것입니다.

[Disclaimer](#)

치의학박사학위논문

**Detailed canal morphology comparison of
micro-computed tomography and clearing technique
in permanent first molar mesiobuccal and mesial roots**

상하악 제1대구치 근심협측치근과 근심치근에서의
미세전산화 단층촬영과 치아투명화 방법을 이용한
미세 근관 형태 비교

2015년 2월

서울대학교 대학원
치 의 과 학 과 치 과 보 존 학 전 공
김 예 은

Abstract

Detailed canal morphology comparison of micro-computed tomography and clearing technique in permanent first molar mesial and mesiobuccal roots

Yeun Kim

Program in Conservative Dentistry

Department of Dental Science

Graduate School, Seoul National University

(Directed by Prof. Kee-Yeon Kum, D.D.S., M.S.D., Ph.D.)

Objectives.

Micro-computed tomography (MCT) with alternative image reformatting techniques shows complex and detailed root canal anatomy. This study compared the MCT images reconstructed by two-dimensional (2D) thin-slab minimum intensity projection (TS-MinIP) and three-dimensional (3D) volume-rendering technique with the images obtained from the clearing technique, to study detailed root canal morphology in maxillary first molar mesiobuccal (MB) roots and mandibular first molar mesial (MS) roots.

Methods.

Extracted human maxillary first molar MB roots (n = 18) and mandibular first molar MS roots (n = 31) were scanned by MCT (Skyscan 1172). The MCT images were constructed using 2D TS-MinIP and 3D volume-rendering technique. The same teeth were then processed by the clearing technique and the clearing images were obtained. For each root, the clearing, the 2D TS-MinIP, the 3D volume-rendered, and the combined 2D TS-MinIP and 3D volume-rendered images were examined independently by 4 dentists and categorized according to Vertucci's classification. Fine anatomical structures such as accessory canals, intercanal communications, and loops were also compared.

Results.

Complex canal systems were more clearly visible in the MCT images than the clearing images. On each root, the 3 MCT images showed the same canal configuration, whereas the clearing images showed less complicated configuration than the MCT ones. The frequency of non-classifiable configurations by Vertucci's classification was shown as 38.9% in maxillary first molar MB roots and 51.6% in mandibular first molar MS roots. Fine anatomical structures such as intercanal communications, accessory canals, and loops were mostly found with the combined 2D TS-MinIP and 3D volume-rendered images.

Conclusions.

The combined 2D TS-MinIP and 3D volume-rendered images of MCT could be useful for morphological study of complex root canal systems. In the future, the establishment of a systematic classification that embraces non-classifiable canal configurations found in this study may help the root canal morphological study.

Keywords: Canal configuration, clearing technique, micro-computed tomography, minimum intensity projection, Vertucci's classification, volume rendering

Student number: 2011-31163

Contents

Abstract	
I. Introduction	1
II. Materials and Methods	6
III. Results	13
IV. Discussion	17
V. References	27
Tables and Figures	33
Abstract in Korean	52

Detailed canal morphology comparison of micro-computed tomography and clearing technique in permanent first molar mesial and mesiobuccal roots

Yeun Kim, D.D.S., M.S.D.

Program in Conservative Dentistry

Department of Dental Science

Graduate School, Seoul National University

(Directed by Prof. Kee-Yeon Kum, D.D.S., M.S.D., Ph.D.)

I. Introduction

Along with diagnosis and treatment planning, knowledge of the root canal morphology is a basic prerequisite for endodontic success (1). Anatomical variations and complexities of the root canal system especially pose challenges to endodontic treatment. Accordingly, the canal morphology of maxillary first molar mesiobuccal (MB) roots has been widely studied because of the prevalence of additional canals and complex configurations (2-4). Likewise, mandibular first molar mesial (MS) roots canal morphology has been researched due to complex canal anatomy including intercanal communications and isthmuses (5), and lower rates of success with

endodontic treatment (6). Additionally, being the first permanent teeth to erupt, permanent first molars are the most frequently in need of endodontic treatment by the clinicians (7). These anatomical complexities and frequent treatments of permanent first molars have read a lot of researches on MB and MS root canal morphology (2-5,8-22).

For the root canal anatomical studies, the classification systems have been proposed and used since Weine *et al.* (2) reported 4 canal configurations using conventional radiograph with file insertion by *in vivo*. Weine's classification has only 4 basic types, so it made clinicians to understand the root canal morphology more simply. However, this system has shown the limitation that could not describe complex root canal configurations, therefore Vertucci (8) suggested root canal classification system composed of 8 canal configurations by observing 100 teeth *in vitro* using clearing technique. After that, even though non-classifiable configurations that were not comprised in Vertucci's classification have been reported, Vertucci's classification have been used as criteria in many studies including the present study, whether additional types is included or not (5,9-22).

Certain factors could contribute to the wide variations reported in the canal morphology. These variations in canal morphology might be attributed to multiple factors, including racial divergence, age, gender, number of the subject or teeth, as well as the study design (clinical or laboratory) (4,5,9-35).

The laboratory methods used to analyze root canal morphology include clearing technique, plastic, or metal castings, *in vitro* endodontic

access with radiography and instruments or instruments only, *in vitro* radiopaque gel infusion and radiography, *in vitro* root canal treatment, *in vitro* radiography, *in vitro* macroscopic examination, scanning electron microscope examination of pulp floor, and grinding or sectioning (4,5,8-18).

The techniques used in clinical studies include inspection during endodontic treatment with or without magnification tools, radiography, and reviews of patient records (3-5). Currently, technologic advances have been developed allowing a study that is accurate and nondestructive, like computed tomography, spiral computed tomography, micro-computed tomography (MCT), and cone-beam computed tomography (CBCT) (19-34).

Among these various techniques, the clearing technique has been used as the gold standard for studying root canal anatomy in earlier studies. However, the clearing technique is destructive, can distort internal anatomy and create artifacts (36). Furthermore, as a long history, the clearing technique has various modifications according to researchers, including change of experimental sequence, different processing time and temperature, different concentration of solution, and different injection material like India ink, Chinese ink, and hematoxylin dye (8-18). These changes of experimental conditions could influence not only the tooth conditions, but also the result of studies (36).

Recently, these shortcomings have now been overcome by MCT that provides detailed visualizations of internal and external root canal anatomy in a non-destructive process (19-30). Moreover, using the same raw dataset from

MCT scanning, the MCT analysis can be further enhanced just by utilizing different image reformatting techniques to visualize more detailed anatomy, like two-dimensional (2D) thin-slab minimum intensity projection (TS-MinIP) and three-dimensional (3D) volume-rendering.

A curved TS-MinIP technique, providing a 2D view of ray projection perpendicular to the axis of the target, is an image reformatting method used widely in medical research and diagnosis but rarely used in dental field. This enables the detection of low-density structures within a given volume to visualize not only airways, ducts, vessels (37,38), but also root canals of fine diameter (19). The greatest advantage of the 2D TS-MinIP image is that low-density structures are emphasized contrary to surrounding high-density structures, like bone, dentine, and so on. However, the 3D direction of the exit or the location of the apical foramen and accessory canals could rarely be observed.

On the other hand, the 3D volume-rendered image of canal with MCT data shows spatial relationship among canal structures. Recent MCT studies suggested that 3D modeling analysis made it possible to study the anatomy more accurately while overcoming the shortcomings of earlier morphological studies (19-30). The advantage of the 3D volume-rendered over the 2D TS-MinIP is that this image could visualize the small accessory canals and minute root canal structures without missing. However, the fine low-density structures could be less distinctively observed in 3D volume-rendered image than in 2D TS-MinIP one.

The previous study showed that the 2D TS-MinIP together with the 3D volume-rendered images of MCT provided the best visualization of detailed canal structures like intercanal communications, loops and accessory canals in maxillary molar MB roots (19). That is, the combined 2D TS-MinIP and 3D volume-rendered images were useful than the 2D TS-MinIP images or the 3D volume-rendered images alone.

The aim of the present study was to compare the 2D TS-MinIP, the 3D volume-rendered, and the combined 2D TS-MinIP and 3D volume-rendered images from MCT with the images obtained from the clearing technique (the clearing image) to study detailed root canal morphology in maxillary first molar MB roots and mandibular first molar MS roots.

II. Materials and Methods

The flow chart of materials and methods is represented in Figure 1.

Sample preparation

Approval was obtained from the Institutional Review Board (IRB) of Seoul National University Dental Hospital, Seoul, Korea (ERI 12006 and ERI 12007). Maxillary and mandibular first molars with closed apexes that had been extracted due to prosthodontic and periodontal reasons from were examined with periapical radiographs. Teeth with a single canal were excluded, so that maxillary first molar MB and mandibular first molar MS roots with two canals and complex configurations could be studied. Teeth with fractured MB and MS roots, and those previously accessed for initiating root canal treatment were also excluded, so that only unmodified and uninstrumented canal anatomy was studied. Finally, 18 maxillary first molar and 31 mandibular first molar were selected. The selected teeth were immersed to disinfect the surface in 3.5% sodium hypochlorite (Yuhanrox; Yuhan Co., Seoul, Korea) for 1 hour, and any remaining organic residue or calculus were removed mechanically with an ultrasonic scaler and curette. They were then stored in 0.5% sodium azide solution until use.

Reconstruction of 2D TS-MinIP and 3D volume-rendered images

MCT scanning

Each tooth (n = 49) was scanned by MCT (SkyScan 1172; SkyScan b.v.b.a., Aartselaar, Belgium), with a voxel dimension of 15.91 μm using 100 kV, 100 μA , a 0.5 mm thick aluminum filter, by 0.5° increments through 180° of rotation. Each image was included to reconstruct a cross-sectional dataset of the MB and MS root by using NRecon (Version 1.6.4.7; Skyscan NV, Kontich, Belgium) on a personal computer. This cross-sectional dataset was used commonly to create the 2D TS-MinIP and the 3D volume-rendered images of each MB and MS root canal system by using OnDemand3D software (Cybermed Inc., Seoul, Korea), as previously outlined (19).

Reconstruction of 2D TS-MinIP images

The 2D TS-MinIP images of the roots can be constructed using OnDemand3D software with the following procedure (Figure 2). At first, the volume image of the tooth is positioned with the root apex upward. Subsequently, it is rotated so that the more than two canals overlapped as much as possible in the sagittal view. The canal axis is set according to the curvature of the canals. In the sagittal view, the thickness of the slab through which the virtual ray to be transmitted is determined to include the width of the canal. The slab thickness is dependent on the size of the canals and usually range from 0.5 to 1.0 mm.

Using OnDemand3D software, a virtual ray is transmitted orthogonal to the curved slab, and the smallest gray value is recorded to obtain the 2D TS-MinIP image (19).

Reconstruction of 3D volume-rendered images

With the same cross-sectional dataset, the OnDemand3D volume rendering tool was used with thresholding and manual volume segmentation to create the 3D volume-rendered images. Additionally, segmented volumes of canal structure were represented by an opaque red color and the external morphology of the MB and MS root was rendered transparent so as to enhance the visualization of fine anatomical structures (Figure 3).

Combination of 2D TS-MinIP and 3D volume-rendered images

For the combined 2D TS-MinIP and 3D volume-rendered images, two types of images were observed concurrently (Figure 4).

Clearing and staining technique

Maxillary first molar MB roots

The teeth were accessed and #10K files (Mani Inc., Tochigi, Japan) were placed in the MB canals to the apical foramen. They were then immersed in 5% sodium hypochlorite (Showa Co., Tokyo, Japan) for 12 hours at room temperature to dissolve pulp tissue and organic debris. This was followed by placement under running tap water for 4 hours to wash away the hypochlorite

and remaining debris.

The teeth were then decalcified and rendered transparent using methods adopted from Robertson *et al* (36). They were decalcified in 5% nitric acid (Sigma-Aldrich Co., St. Louis, MO, USA) at room temperature, agitated by hand twice a day, and placed in fresh acid solution every 2 days over a period of 5 days. They were then placed under running tap water for 2 hours and immersed in acetic acid (Sigma-Aldrich Co.) for 24 hours. Thereafter, the decalcified teeth were sequentially dehydrated in ascending concentrations of ethanol (70%-12 hours, 90%-6 hours, and 100%-6 hours). They were then placed in a methyl salicylate solution (Sigma-Aldrich Co.) for 24 hours which cleared and hardened the specimens. Finally, India ink (Higgins Fountain India Ink, Tampa, FL, USA) was applied to visualize the root canal systems. India ink was injected into the pulp chamber with a 27-gauge needle on a disposable syringe. Then, the ink was drawn through the canal system by applying negative pressure at the apical end of the tooth with a suction tip attached to the root apex and connected to the centralized vacuum system. Excess ink was removed with ethanol and a brush. After resecting the distobuccal and palatal roots, the MB root was photographed with a dissecting microscope (5X magnification; Olympus, Tokyo, Japan).

Mandibular first molar MS roots

After access preparation, #10 K-files were inserted into the MS root canals through their apical foramina. In contrast with maxillary first molar, the distal

root of mandibular first molar was resected in early stage with a high speed diamond bur. The teeth were then placed in 5% sodium hypochlorite only for 2 hours dissolve pulp tissue and organic residue followed by rinsing under running tap water for 4 hours to remove the sodium hypochlorite and dissolved debris. The opening into the pulp chamber from the distal root resection was sealed with flowable resin (Denfil flow; Varicom Co. Ltd., Seoul, Korea). The MS root canals were injected with India ink using a 27-gauge needle on a disposable syringe placed through the pulp chamber. Negative pressure from a suction tip was applied to the apical foramina. Additional India ink was injected into the pulp chamber and the access opening was sealed with utility wax. Then the teeth were decalcified in 5% nitric acid for 3 days with a change of new solution after 12 hours. The decalcified teeth were washed under running tap water for 2 hours. Finally the decalcified teeth were dehydrated gradually in ascending concentrations of ethanol (as same as above) and placed in methyl salicylate solution for 24 hours to clear and harden the specimens. The cleared and stained MS roots were photographed under a dissecting microscope.

Classification of canal configurations and fine structures

For each MB and MS root (n = 49), the clearing, the 2D TS-MinIP, the 3D volume-rendered, and the combined 2D TS-MinIP and 3D volume-rendered images were prepared independently (Figure 4). Each root canal system was carefully examined and categorized independently by 4 dentists using the

Vertucci's classification systems (8) as follows (Figure 5). All 4 dentists agreed on the canal configuration after deliberation of differences.

- Vertucci type I. One canal extends from the pulp chamber to the apex.
- Vertucci type II. Two separate canals leave the pulp chamber and join short of the apex to form one canal.
- Vertucci type III. One canal leaves the pulp chamber, divides into two within the root, and then merges to exit as one canal.
- Vertucci type IV. Two separate and distinct canals extend from the pulp chamber to the apex.
- Vertucci type V. One canal leaves the pulp chamber and divides short of the apex into two separate and distinct canals with separate apical foramina.
- Vertucci type VI. Two separate canals leave the pulp chamber, merge in the body of the root, then divide short of the apex and exit as two distinct canals.
- Vertucci type VII. One canal leaves the pulp chamber, divides and then merges within the body of the root, and finally divides into two distinct canals short of the apex.
- Vertucci type VIII. Three separate and distinct canals extend from the pulp chamber to the apex.

The descriptions of main canals, as well as accessory canals,

intercanal communications and loops were based on the terminology provided by Vertucci (1). Main canals are the root canals from the chamber orifice to the apex. Accessory canals are defined as any branch of the main canals or chamber that communicates with the external surface of the root. Intercanal communication was defined extensively as a branch of the pulpal space that runs between the main canals but does not communicate with the root surface. Especially, since the definition of intercanal communication is so broad and could influence the classification of root canal system, the intercanal communication was defined as narrow bands which have smaller than half diameters of main canals in the present study. Furthermore, those configurations that did not fit into Vertucci's classification system (8) were categorized as non-classifiable.

Interobserver agreement amongst the 4 dentists for the 4 images was assessed independently using Fleiss kappa (39), which is statistically significant when the coefficient is greater than 0.7. Disagreements between observers were discussed to reach consensus. When all 4 images of a root canal system were categorized as having the same configuration, the images were deemed to be in agreement on the classification. Additionally, the incidence and location of accessory canals, intercanal communications, and loops that were detected by the 4 images were compared.

III. Result

Classification of canal configurations

Maxillary first molar MB roots

In canal classification, there was no difference between the 3 MCT images, that were the 2D TS-MinIP, the 3D volume-rendered, and the combined 2D TS-MinIP and 3D volume-rendered. However, the agreement in their classification among the 4 images including the clearing images was only 33.3% (6/18) due to the difference between the clearing images and the 3 MCT images (Table 1).

In the clearing images, Vertucci's type I was the most frequent configuration. The non-classifiable configurations were the most frequent in the 3 MCT images, followed by Vertucci's type VI (Table 2).

Specifically, seven (38.9%) MB roots shown as Vertucci's type I in the clearing images, were classified to Vertucci's type IV (1/7), type VI (3/7), or non-classifiable (3/7) in the 3 MCT images (Table 1). An example was shown in Figures 8E, 8F, and 8G. On each MB root that showed disagreement among the 4 images, the number of Vertucci's type in the clearing image was less than that in the 3 MCT images (Table 1).

Seven (38.9%) MB roots on the MCT images had 5 non-classifiable configuration types that are not included in Vertucci's classification. These were types 1-2-1-3, 2-1-2-1-2, 2-3, 2-3-4-3-2, and 3-2-1-2. The representative

examples were shown in Figure 6. Among these, one configuration (type 3-2-1-2) was the first to be reported in maxillary first molar MB roots. Any new canal configuration was not found in the clearing images. Overall, canal configuration types and multiple canals were more clearly described in the MCT images than in the clearing ones.

Meanwhile, when classifying canals, there was a high level of interobserver agreement among the 4 dentists, with Fleiss kappa coefficients of 0.874, 0.791, 0.829, and 0.829 for the clearing, the 2D TS-MinIP, the 3D volume-rendered, and the combined 2D TS-MinIP and 3D volume-rendered images, respectively. (The each data by 4 dentists was omitted.)

Mandibular first molar MS roots

In canal classification, there was no difference between the 3 MCT images. However, all 4 images resulted in agreement on the Vertucci's classification for 45.2% (14/31) of the roots due to the difference between the clearing images and the 3 MCT ones (Table 3).

Specially, five (16.1%) MS roots, classified to Vertucci's type IV (4/5) and VIII (1/5) in the clearing images, were found as non-classifiable by the 3 MCT images. On each MS root that showed disagreement among the 4 images, the number of Vertucci's type in the clearing image was less than that in the 3 MCT images (Table 3).

Regardless of the technique, non-classifiable configurations were the most frequent in these MS roots that had multiple canals, followed by

Vertucci's type IV, and type II (Table 4).

Sixteen (51.6%) MS roots on the MCT images had 10 non-classifiable configuration types that are not included in Vertucci's classification. These were types 1-3-1, 2-1-2-3, 2-1-3-2, 2-3, 2-3-2, 2-3-5, 3-2, 3-2-1, 3-4-3, and 3-4-3-4. The representative examples were shown in Figure 7. Among these, six configurations (types 1-3-1, 2-1-2-3, 2-1-3-2, 2-3-5, 3-4-3, and 3-4-3-4) were the first to be reported in mandibular first molar MS roots. Three new configurations (types 2-1-3-2, 2-3-5, and 3-4-3) were not found in the clearing images.

Meanwhile, for the classification of canal configurations there was substantial interobserver agreement between the 4 dentists. Their Fleiss kappa coefficients were 0.736, 0.705, 0.712, and 0.712 for the clearing, the 2D TS-MinIP, the 3D volume-rendered, and the combined 2D TS-MinIP and 3D volume-rendered images respectively. (The each data by 4 dentists was omitted.)

Identification of fine anatomical structures

Maxillary first molar MB roots

Fine anatomical structures such as accessory canals, intercanal communications, and loops were identified in the clearing (3, 1, and 3, respectively), in the 2D TS-MinIP (31, 22, and 15), in the 3D volume-rendered (40, 15, and 12), and in the combined 2D TS-MinIP and 3D volume-rendered images (43, 23, and 15) (Table 5).

Intercanal communications and loops found in the clearing images were all located in the middle third of the root. In the 3 MCT images, intercanal communications and loops were identified in the cervical and apical thirds, as well as the middle third (Table 5).

Detailed anatomical structures were more clearly observed in the MCT images than the clearing ones (Figure 8). Fine canals were more visible in the 2D TS-MinIP images (Figure 8J), and accessory canals that were hidden by the main canal could be visible in the 3D volume-rendered ones (Figures 8K and 8L).

Mandibular first molar MS roots

Fine anatomical structures such as accessory canals, intercanal communications, and loops were identified in the clearing (13, 60, and 10, respectively), in the 2D TS-MinIP (20, 70, and 13), in the 3D volume-rendered (20, 49, and 13), and in the combined 2D TS-MinIP and 3D volume-rendered images (24, 71, and 17) (Table 6).

Fine anatomical structures such as the intercanal communications and loops that were located in the coronal and middle third were more clearly observed in the 2D TS-MinIP images than the clearing ones (Figures 9A, 9B, and 9C). On the contrary, accessory canals were more clearly observed in the 3D volume-rendered images than the 2D TS-MinIP ones (Figures 9E, 9F and 9G).

IV. Discussion

Until recently the clearing technique served as the gold standard for studying root canal anatomy *in vitro* (8-18). Now MCT is becoming a standard method that overcomes limitations in the clearing technique (19-30). Eder *et al.* (40) reported that MCT could describe the exact canal configuration, verify information identical to histology, and thus serve as the “gold standard” *in vitro* morphology study. Furthermore, a recent study (19) showed that complex canal configurations and fine anatomical structures are more readily observed by MCT, when the 2D TS-MinIP image could serve as an adjunct to the 3D volume-rendered image for canal morphology study. However, the previous studies did not directly compare these images with the clearing image (8-18). The absence of the gold standard as a control meant that the presence of false positives and negatives in canal morphology could not be clearly identified. These limitations were overcome in our study by comparing the 2D TS-MinIP, the 3D volume-rendered, and the combined 2D TS-MinIP and 3D volume-rendered images by MCT with the clearing image. The present study showed the superiority of combining the 2D TS-MinIP images with the 3D volume-rendered ones by MCT to identify fine anatomical features and canal configurations in the maxillary first molar MB roots and mandibular first molar MS roots.

Through several studies (19-30), MCT was found to afford much

greater visualization of fine anatomical structures. This was likely due to its greater capacity to distinguish between empty air space and the surrounding dentin through different scales of gray (23,26). Furthermore, the use of different image reformatting techniques with MCT, such as 2D TS-MinIP and 3D volume-rendering, provided better visualization of detailed anatomy. Indeed, the 2D TS-MinIP and the 3D volume-rendered images alone provided the same canal configurations, but when combined, they identified much more fine anatomical structures. Similarly, other studies found that MCT clearly visualizes complex anatomical structures, including the pulp chamber, dentin thickness and canal dimensions (22,28-30).

Therefore to rigorously compare MCT, it was essential that the clearing technique should be optimized. Accordingly, our study included two different methods in the clearing technique that increased the visualization of detailed anatomical structures. The tooth clearing using maxillary first molars was conducted prior to mandibular first molars. The clearing method for maxillary first molars was found to have some limitation to show detailed canal morphology, so the sequence of clearing technique was changed as follows (Figure 1).

At first, the exposed time of 5% sodium hypochlorite was changed from 12 hours to 2 hours, since the teeth treated with 12 hours were physically too fragile to handle. The long exposed time of sodium hypochlorite might dissolve not only the pulp tissue but also the organic material of teeth itself, like collagen and affect the solidity of teeth. For the same reason, the

treatment of acetic acid was omitted in process of mandibular first molars. Actually, the treatment of nitric acid alone was enough to decalcify the teeth.

Again, the maxillary first molar MB root canals were stained just after clearing as referred to the previous studies (11,12,15), while mandibular first molar MS root canals were stained prior to clearing as referred to other studies (9,10,13,14,16,17), so as to enhance ink penetration of fine structures. Since methyl salicylate has low water solubility, its penetration may be reduced in canals that become more hydrophobic after decalcification. Therefore, the method of staining before clearing that was used in mandibular first molars was expected to increase the visualization of anatomical structures in comparison with maxillary first molar.

Indeed, in our study, there was an increase in agreement on the classification of canal configurations in mandibular first molar MS root (45.2%), compared to maxillary first molar MB root (33.3%). In both MB and MS root cases, the combined 2D TS-MinIP and 3D volume-rendered images were the most effective at identifying fine structures, followed by the 2D TS-MinIP alone. However, in case of maxillary first molar, fewer fine anatomic structures were identified in the clearing image than any of the MCT ones, while the clearing images from mandibular MS roots appeared to be a little more effective to show detailed anatomy than the 3D volume-rendering alone in mandibular first molar. Furthermore, in a few roots of mandibular first molar, intercanal communications that were located within the middle and apical sections were more readily visible in the clearing images than the 3D

volume-rendered ones.

Despite these refinements, the clearing technique was found to have several shortcomings. A few of the teeth became too fragile to handle after they were decalcified. In fact, teeth that had been processed through multiple procedures would ultimately disintegrate from mechanical or chemical stimuli. Additionally, India ink would sometimes fail to penetrate canals, which was likely due its strong affinity to proteins retained within their lumen (41). Ultimately, the greatest disadvantage was that the pungent odor irritated our eyes and throats, and the toxicity of methyl salicylate remained a major concern (42).

In our study, Vertucci's classification was chosen to express the complexities of MB and MS root canal configurations, even though this one has also the limitation not to cover all kinds of canal configurations. Since Vertucci suggested a classification that consists of only 8 canal configurations (8), there have been several reports of non-classifiable canal types. After that, Ng *et al.* (9) modified the Vertucci classification by adding seven additional configurations for in-depth morphology study of maxillary molar teeth and found 3 additional configurations (types 2-1-2-1, 3-2, and 2-3) in Burmese maxillary first molars. Alavi *et al.* (10) also found one configuration (type 1-3-1) that was not classifiable by the Vertucci classification in Thai maxillary first molars. In their two morphology studies that used clearing technique in Turkish maxillary first molars, Sert and Bayirli (11) and Sert *et al.* (12) reported two (types 3-2-1 and 2-3-2-1-2) and three (types 1-2-3-2, 2-3, and 2-

1-2-1) new configurations that were not included in the Vertucci classification, respectively. Recently, Gu *et al.* (19) and Kim *et al.* (21) in their MCT studies reported six (types 1-2-1-2-1, 1-2-1-3, 2-1-2-1-2, 2-1-3, 3-2-1, and 3-2-1-2-1) and three (types 1-3, 2-3-2-3-2, and 2-3-4-3-2) new configurations in maxillary first molars, respectively, that were not classifiable by the Vertucci classification. The present MCT study also found 5 non-classifiable configuration types in maxillary first molar that were not included in the Vertucci classification. Moreover, among these, one configuration (type 3-2-1-2) has never been reported for maxillary first molar MB roots.

The reports of non-classifiable canal types for mandibular first molar MS roots are as follows. Gulabivala *et al.* (13,14) reported 4 additional canal configurations (types 2-1-2-1, 2-3, 3-1, and 3-2) in Burmese mandibular first molar MS roots and one (type 3-4) in Thai mandibular first molars. Sert *et al.* (11,15) and Peiris *et al.* (16) reported one (type 1-2-3-2) and two (types 1-2-3 and 3-1-2) new canal configurations in Turkish and Sri Lankan mandibular first molar MS roots, respectively. Al-Qudah and Awawdeh (17) also reported additional configurations (types 2-3-1, 2-3-2, 3-2-1, and 3-2-3) in Jordanian mandibular first molar MS roots. Chen *et al.* (18) reported a new configuration (type 2-3-1-2) in Taiwanese mandibular first molars. In another succeeding study, Sert *et al.* (12) reported two (types 2-3-4-2 and 3-1-2-1-2) new canal configuration in Turkish mandibular first molar MS roots. Likewise, the present study found 10 non-classifiable canal configurations that are not included in Vertucci's classification in mandibular first molar MS roots,

respectively. Among these, six canal configurations (types 1-3-1, 2-1-2-3, 2-1-3-2, 2-3-5, 3-4-3, and 3-4-3-4) have not previously been reported in mandibular first molar MS roots.

These frequencies of non-classifiable configurations demonstrated the complexity of permanent first molar MB and MS root canal anatomy. Furthermore, it showed that the present classification system has limitations in encompassing the variety of root canal configurations. Therefore the development of a systematic classification that embraces these complex canal configurations could advance the field.

However, the high frequency (38.9% in maxillary first molar MB roots and 51.6% in mandibular first molar MS roots) of complex and non-classifiable configurations reported in this study may have been due to the non-random process for selecting the teeth. The MB and MS roots with at least two radiographically visible canals were intentionally chosen so as to compare the different techniques for studying canal morphology. Furthermore, these teeth had been extracted for prosthodontic and periodontal reasons from older patients, in whom dentin accumulation within the canals may have contributed to the complexity of the configurations seen (35). Therefore these limitations along with the sample size and the patient age mean that the high frequency of non-classifiable canal configurations may not be as prevalent in the general population (35).

In case of maxillary first molar MB roots (Table 5), the MCT images showed intercanal communications that were mostly located in the middle

third of the root, which is consistent with other recent MCT studies (19,20,27). They also showed a high prevalence of accessory canals in the apical region, which is also consistent with previous studies (8,19,20,27). Indeed, the 3 MCT images showed that all 18 MB roots (100%) had multiple canals, whereas the clearing images revealed that only 11 of these (61.1%) had additional canals. This failure of the clearing images may have been due to limited dye penetration in small, delicate, and calcified canals (Figure 8E).

In case of mandibular first molar MS roots, except non-classifiable through all of these images, the most common canal configuration was Vertucci's type IV, followed by type II, which is consistent with previous studies of mandibular first molar anatomy (5,13,14,22,30). The accessory canals were found mostly (95.8%) in the apical third (Table 6), which is also consistent with prior findings (22,30). Additionally, the high incidence (80.6%) of intercanal communications in these mandibular first molar MS roots (Table 6) has also been reported recently (5,29,30).

Furthermore, in both cases of maxillary first molar MB and mandibular first molar MS roots, fewer accessory canals were identified in the 2D TS-MinIP images than the other MCT ones because of its limitation in reproducing the 3D position of accessory canals within the root canal system (Table 6). However, the combined 2D TS-MinIP and 3D volume-rendered images showed the most accessory canals, intercanal communications, and loops because they compensated for the limitations of each technique. Indeed, this combined 2D TS-MinIP and 3D volume-rendered images should be

exploited for studying detailed canal morphology.

Therefore, despite the advantages of the 2D TS-MinIP technique in visualizing fine and intricate canal structures, an understanding of the flaws and limitations of the method is essential for an accurate evaluation of this image reformatting technique. It records the smallest gray value for the path of a ray passing through a slab of image, so that air or low attenuated structures are emphasized in contrast to surrounding high attenuated structures. Even when anatomic structures are tortuous or twisted, in the 2D TS-MinIP images, the lumen is seen as patent and continuous. However, depending on the direction of beam projection, overlapping minute canals may be missed, and the 3D direction of the exit or the location of the apical foramen, accessory and lateral canals may be difficult to observe, when compared with the 3D volume-rendered image (19). In addition, if the slab extends beyond the root surface because of a root concavity or severe curvature, the pixel value from outside the root is recognized as the minimum value (43) and thereby creates a pseudo-canal image (44). Therefore, in our study, thin slabs of the target area were appropriately set by using information from axial, coronal, and sagittal images, minimizing any chance of false-positive canals such as pseudo-lumen.

However, because the 3D volume-rendered images alone were somewhat deficient in detecting small, calcified, or faint root canals, it is the combined 2D TS-MinIP and 3D volume-rendered images that may be the most useful for the in-depth morphology study of complex root canal systems.

In the present study, the incidence of unclassifiable canal configurations was higher for all 3 MCT images than with the clearing ones (Tables 2 and 4). This showed the accuracy of the MCT images, and that using the combined 2D TS-MinIP and 3D volume-rendered images was the most sensitive method for studying in-depth morphology. However, despite the enhanced accuracy and nondestructive nature of MCT compared with the conventional clearing technique, both techniques are limited to *in vitro* application. Therefore, a method that has the accuracy of MCT and is also clinically feasible would be highly beneficial for endodontic practice (31).

Recently, some studies of canal anatomy that used CBCT (32-34) showed that there are several advantages for *in vivo* techniques, compared with *in vitro* methods that use extracted teeth. These CBCT images show fewer fine anatomic structures but still provide clinically useful information. For example, an *ex vivo* study by Domard *et al.* (34) found that the canal counts with CBCT were not significantly different from MCT in the MB root of maxillary molars. Furthermore, there is the possibility that CBCT could be used for the clinical application of the 2D TS-MinIP techniques. Although the resolution of clinically used CBCT reaches 76 μm , which is around five-fold the value for MCT in the present study, ongoing technical advances are likely to narrow this gap (34). In addition, the reformatting method for visualizing canals in the 2D TS-MinIP is relatively simple, compared with that for the 3D volume-rendering when using CBCT data. For the 3D volume-rendering technique, all structures adjacent to the canal need to be removed in a time-

consuming process, whereas for the 2D TS-MinIP technique, the clinician positions the target tooth and simply defines the slab along the canal. Therefore, in the future it is likely that the 2D TS-MinIP technique may also be used *in vivo* to study canal morphology.

Although the clearing technique is considered the gold standard for studying root canal morphology *ex vivo*, complex MB and MS root canal systems of permanent first molars could not be fully revealed by this technique alone.

Under the limitation of the present study, Canal configurations and fine anatomical structures were more clearly observed in the combined 2D TS-MinIP and 3D volume-rendered images of MCT than the clearing images. Also, the Vertucci's classification has limitations in encompassing the variety of canal configurations observed in the permanent first molar MB and MS roots. Therefore the establishment of a systematic classification that embraces these complex canal configurations could advance the field.

V. References

1. Vertucci FJ. Root canal morphology and its relationship to endodontic procedures. *Endod Topics* 2005;10:3-29.
2. Weine FS, Healey HJ, Gerstein H, Evanson L. Canal configuration in the mesiobuccal root of the maxillary first molar and its endodontic significance. *Oral Surg Oral Med Oral Pathol* 1969;28:419-425.
3. Stropko JJ. Canal morphology of maxillary molar: clinical observations of canal configuration. *J Endod* 1999;25:446-450.
4. Cleghorn BM, Christie WH, Dong CCS. Root and root canal morphology of the human permanent maxillary first molar: a literature review. *J Endod* 2006;32:813-821.
5. de Pablo OV, Estevez R, Péix Sánchez M, Heilborn C, Cohenca N. Root anatomy and canal configuration of the permanent mandibular first molar: a systematic review. *J Endod* 2010;36:1919-1931.
6. Swartz DB, Skidmore AE, Griffin JA Jr. Twenty years of endodontic success and failure. *J Endod* 1983;9:198-202.
7. Scavo R, Martinez Lalis R, Zmener O, Dipietro S, Grana D, Pameijer CH. Frequency and distribution of teeth requiring endodontic therapy in an Argentine population attending a specialty clinic in endodontics. *Int Dent J* 2011;61:257-260.
8. Vertucci FJ. Root canal anatomy of the human permanent teeth. *Oral*

Surg Oral Med Oral Pathol 1984;58:589-599.

9. Ng YL, Aung TH, Alavi A, Gulabivala K. Root and canal morphology of Burmese maxillary molars. *Int Endod J* 2001;34:620-630.
10. Alavi AM, Opananon A, Ng YL, Gulabivala K. Root and canal morphology of Thai maxillary molars. *Int Endod J* 2002;35:478-485.
11. Sert S, Bayirli GS. Evaluation of the root canal configurations of the mandibular and maxillary permanent teeth by gender in the Turkish population. *J Endod* 2004;30:391-398.
12. Sert S, Şahinkesen G, Topçu FT, Eroğlu SE, Oktay EA. Root canal configurations of third molar teeth. A comparison with first and second molars in the Turkish population. *Aust Endod J* 2011;37:109-117.
13. Gulabivala K, Aung TH, Alavi A, Ng YL. Root and canal morphology of Burmese mandibular molars. *Int Endod J* 2001;34:359-370.
14. Gulabivala K, Opananon A, Ng YL, Alavi A. Root and canal morphology of Thai mandibular molars. *Int Endod J* 2002;35:56-62.
15. Sert S, Aslanalp V, Tanalp J. Investigation of the root canal configurations of mandibular permanent teeth in the Turkish population. *Int Endod J* 2004;37:494-499.
16. Peiris R, Takahashi M, Sasaki K, Kanazawa E. Root and canal morphology of permanent mandibular molars in a Sri Lankan population. *Odontology* 2007;95:16-23.
17. Al-Qudah AA, Awawdeh LA. Root and canal morphology of mandibular first and second molar teeth in a Jordanian population. *Int*

- Endod J* 2009;42:775-784.
18. Chen G, Yao H, Tong C. Investigation of the root canal configuration of mandibular first molars in a Taiwan Chinese population. *Int Endod J* 2009;42:1044-1049.
 19. Gu Y, Lee JK, Spångberg LS, Lee Y, Park CM, Seo DG, Chang SW, Hur MS, Hong ST, Kum KY. Minimum-intensity projection for in-depth morphology study of mesiobuccal root. *Oral Surg Oral Med Oral Pathol Oral Radiol Endod* 2011;112:671-677.
 20. Verma P, Love RM. A Micro CT study of the mesiobuccal root canal morphology of the maxillary first molar tooth. *Int Endod J* 2010;44:210-217.
 21. Kim Y, Chang SW, Lee JK, Chen IP, Kaufman B, Jiang J, Cha BY, Zhu Q, Safavi KE, Kum KY. A micro-computed tomography study of canal configuration of multiple-canal mesiobuccal root of maxillary first molar. *Clin Oral Investig* 2013;17:1541-1546.
 22. Gu Y, Lu Q, Wang H, Ding Y, Wang P, Ni L. Root canal morphology of permanent three-rooted mandibular first molars--part I: pulp floor and root canal system. *J Endod* 2010;36:990-994.
 23. Rhodes JS, Ford TR, Lynch JA, Liepins PJ, Curtis RV. Micro-computed tomography: a new tool for experimental endodontology. *Int Endod J* 1999;32:165-170.
 24. Bjørndal L, Carlsen O, Thuesen G, Darvann T, Kreiborg S. External and internal macromorphology in 3D-reconstructed maxillary molars

- using computerized X-ray micro-tomography. *Int Endod J* 1999;32:3-9.
25. Peters OA, Laib A, Rueggegger P, Barbakow F. Three-dimensional analysis of root canal geometry by high-resolution computed tomography. *J Dent Res* 2000;79:1405-1409.
26. Plotino G, Grande NM, Pecci R, Bedini R, Pameijer CH, Somma F. Three-dimensional imaging using microcomputed tomography for studying tooth macromorphology. *J Am Dent Assoc* 2006;137:1555-1561.
27. Somma F, Leoni D, Plotino G, Grande NM, Plasschaert A. Root canal morphology of the mesiobuccal root of maxillary first molars: a micro-computed tomographic analysis. *Int Endod J* 2009;42:165-174.
28. Villas-Bôas MH, Bernardineli N, Cavenago BC, Marciano M, Del Carpio-Perochena A, de Moraes IG, Duarte MH, Bramante CM, Ordinola-Zapata R. Micro-computed tomography study of the internal anatomy of mesial root canals of mandibular molars. *J Endod* 2011;37:1682-1686.
29. Versiani MA, Pecora JD, de Sousa-Neto MD. Root and root canal morphology of four-rooted maxillary second molars: a micro-computed tomography study. *J Endod* 2012;38:977-982.
30. Harris SP, Bowles WR, Fok A, McClanahan SB. An anatomic investigation of the mandibular first molar using micro-computed tomography. *J Endod* 2013;39:1374-1378.
31. Neelakantan P, Subbarao C, Subbarao CV. Comparative evaluation of

- modified canal staining and clearing technique, cone-beam computed tomography, peripheral quantitative computed tomography, spiral computed tomography, and plain and contrast medium-enhanced digital radiography in studying root canal morphology. *J Endod* 2010;36:1547-1551.
32. Reis AG, Grazziotin-Soares R, Barletta FB, Fontanella VR, Mahl CR. Second canal in mesiobuccal root of maxillary molars is correlated with root third and patient age: a cone-beam computed tomographic study. *J Endod* 2013;39:588-592.
 33. Kim Y, Lee SJ, Woo J. Morphology of maxillary first and second molars analyzed by cone-beam computed tomography in a Korean population: variations in the number of roots and canals and the incidence of fusion. *J Endod* 2012;38:1063-1068.
 34. Domark JD, Hatton JF, Benison RP, Hildebolt CF. An *ex vivo* comparison of digital radiography and cone-beam and micro computed tomography in the detection of the number of canals in the mesiobuccal roots of maxillary molars. *J Endod* 2013;39:901-905.
 35. Peiris HR, Pitakotuwage TN, Takahashi M, Sasaki K, Kanazawa E. Root canal morphology of mandibular permanent molars at different ages. *Int Endod J* 2008;41:828-835.
 36. Robertson D, Leeb IJ, McKee M, Brewer E. A clearing technique for the study of root canal systems. *J Endod* 1980;6:421-424.
 37. Park SJ, Han JK, Kim TK, Choi BI. Three-dimensional spiral CT

- cholangiography with minimum intensity projection in patients with suspected obstructive biliary disease: comparison with percutaneous transhepatic cholangiography. *Abdom Imaging* 2001;26:281-286.
38. Satoh S, Ohdama S, Shibuya H. Sliding thin slab, minimum intensity projection imaging for objective analysis of emphysema. *Radiat Med* 2006;24:415-421.
 39. Carletta J. Assessing agreement on classification tasks: The kappa statistic. *Comput Linguist* 1996;22:249-254.
 40. Eder A, Kantor M, Nell A, Moser T, Gahleitner A, Schedle A, Sperr W. Root canal system in the mesiobuccal root of the maxillary first molar: an *in vitro* comparison study of computed tomography and histology. *Dentomaxillofac Radiol* 2006;35:175-177.
 41. Hancock K, Tsang VCW. India ink staining of proteins on nitrocellulose paper. *Anal Biochem* 1983;133:157-162.
 42. Lapczynski A, Jones L, McGinty D, Bhatia SP, Letizia CS, Api AM. Fragrance material review on methyl salicylate. *Food Chem Toxicol* 2007;45 Suppl 1:428-452.
 43. William EL, Harvey EC. Marching cubes: A high resolution 3-D surface construction algorithm. *Comp Graph* 1987;21:163-169.
 44. Chang SW, Lee JK, Lee KW, Kum KY. In-depth morphological study of mesiobuccal root canal systems in maxillary first molars: Review. *Restor Dent Endod* 2013;38:2-10.

Table 1. Types of canal configurations of each maxillary first molar MB root classified according to the Vertucci's classification.

Specimen #	Clearing	2D MinIP	3D volume	2D MinIP+3D volume
1	TypeV	TypeV	TypeV	Type V
2	Type II	NC	NC	NC
3	Type VI	Type VI	TypeVI	Type VI
4	NC	NC	NC	NC
5	Type III	TypeVII	Type VII	Type VII
6	Type V	Type V	Type V	Type V
7	Type I	Type VI	Type VI	Type VI
8	Type III	Type III	Type III	Type III
9	Type V	NC	NC	NC
10	Type I	Type IV	Type IV	Type IV
11	Type IV	Type IV	Type IV	Type IV
12	Type I	NC	NC	NC
13	NC	NC	NC	NC
14	Type I	NC	NC	NC
15	Type I	Type VI	Type VI	Type VI
16	Type I	NC	NC	NC
17	Type V	Type V	Type V	Type V
18	Type I	TypeVI	Type VI	Type VI

NC* Non-classifiable

Table 2. Incidence of canal configurations of 18 maxillary first molar MB roots classified according to the Vertucci's classification.

	Type of canal configuration							
	Type I	Type II	Type III	Type IV	Type V	Type VI	Type VII	NC*
Clearing	7 (38.9%)	1 (5.6%)	2 (11.1%)	1 (5.6%)	4 (22.2%)	1 (5.6%)	0 (0%)	2 (11.1%)
2D MinIP	0 (0%)	0 (0%)	1 (5.6%)	2 (11.1%)	3 (16.6%)	4 (22.2%)	1 (5.6%)	7 (38.9%)
3D volume	0 (0%)	0 (0%)	1 (5.6%)	2 (11.1%)	3 (16.6%)	4 (22.2%)	1 (5.6%)	7 (38.9%)
2D MinIP+3D volume	0 (0%)	0 (0%)	1 (5.6%)	2 (11.1%)	3 (16.6%)	4 (22.2%)	1 (5.6%)	7 (38.9%)

NC* Non-classifiable

Table 3. Types of canal configurations of each mandibular first molar MS root classified according to the Vertucci's classification.

Specimen #	Clearing	2D MinIP	3D volume	2D MinIP+3D volume
1	NC	NC	NC	NC
2	TypeV	TypeV	TypeV	TypeV
3	Type IV	Type IV	Type IV	Type IV
4	Type IV	Type IV	Type IV	Type IV
5	Type IV	NC	NC	NC
6	Type VIII	NC	NC	NC
7	Type IV	NC	NC	NC
8	Type IV	Type IV	Type IV	Type IV
9	Type IV	NC	NC	NC
10	Type II	Type II	Type II	Type II
11	NC	NC	NC	NC
12	Type VI	Type VI	Type VI	Type VI
13	NC	NC	NC	NC
14	Type IV	Type IV	Type IV	Type IV
15	NC	NC	NC	NC
16	NC	NC	NC	NC
17	Type IV	Type IV	Type IV	Type IV
18	NC	NC	NC	NC
19	NC	NC	NC	NC
20	NC	NC	NC	NC
21	Type IV	Type IV	Type IV	Type IV
22	TypeV	TypeV	TypeV	TypeV
23	Type II	Type II	Type II	Type II

24	NC	NC	NC	NC
25	Type IV	NC	NC	NC
26	Type II	Type VI	Type VI	Type VI
27	NC	NC	NC	NC
28	Type II	Type II	Type II	Type II
29	Type II	Type II	Type II	Type II
30	Type III	Type III	Type III	Type III
31	NC	NC	NC	NC

NC* Non-classifiable

Table 4. Incidence of canal configurations of 31 mandibular first molar MS roots classified according to the Vertucci's classification.

	Type of canal configuration								
	Type I	Type II	Type III	Type IV	Type V	Type VI	Type VII	TypeVIII	NC*
Clearing	0 (0%)	5 (16.1%)	1 (3.2%)	10 (32.3%)	2 (6.5%)	1 (3.2%)	0 (0%)	1 (3.2%)	11 (35.5%)
2D MinIP	0 (0%)	4 (12.9%)	1 (3.2%)	6 (19.4%)	2 (6.5%)	2 (6.5%)	0 (0%)	0 (0%)	16 (51.6%)
3D volume	0 (0%)	4 (12.9%)	1 (3.2%)	6 (19.4%)	2 (6.5%)	2 (6.5%)	0 (0%)	0 (0%)	16 (51.6%)
2D MinIP+3D volume	0 (0%)	4 (12.9%)	1 (3.2%)	6 (19.4%)	2 (6.5%)	2 (6.5%)	0 (0%)	0 (0%)	16 (51.6%)
NC* Non-classifiable									

Table 5. Numbers and position of accessory canal, intercanal communications, and loops in 18 maxillary first molar MB roots.

Specimen #	Clearing accessory	Clearing intercanal	Clearing loop	2D MinIP accessory	2D MinIP intercanal	2D MinIP loop	3D volume accessory	3D volume intercanal	3D volume loop	2D+3D accessory	2D+3D intercanal	2D+3D loop
1			M1		M1	M1			M1		M1	M1
2												
3					M1		A1	M1		A1	M1	
4					M1		A2			A2	M1	
5			M1	A1	M1	M1	A1	M1	M1	A1	M1	M1
6				A2			A2			A2		
7				A1	M2	C1	A2	M2	C1	A2	M2	C1
8					M2	A1,M1	A1	M1	A1	A1	M2	A1,M1
9					M1,C1	M1		M2			M2,C1	M1
10				A5	M1,C1	M4	A8		M3	A8	M1,C1	M4
11	A1	M1		A2	M2	A1	A4	M1	A1	A4	M2	A1
12				A4	A1,M2,C2		A5	M2,C2		A5	A1,M2,C2	
13	A1		M1	M1		M3			M3	M1		M3
14	A1			A5	M2		A4	M2		A5	M2	
15				A1			A2			A2		
16					M1			M1			M1	
17				A5		A1	A4		A1	A5		A1
18				A4			A4			A4		

total	3	1	3	31	22	15	40	15	12	43	23	15
-------	---	---	---	----	----	----	----	----	----	----	----	----

Letter denotes anatomical position: C, cervical; M, middle; A, apical.
Arabic numeral denotes number of features identified.

Table 6. Position and number of accessory canal, intercanal communications, and loops in 31 mandibular first molar MS roots.

Specimen #	Clearing accessory	Clearing intercanal	Clearing loop	2D MinIP accessory	2D MinIP intercanal	2D MinIP loop	3D volume accessory	3D volume intercanal	3D volume loop	2D+3D accessory	2D+3D intercanal	2D+3D loop
1	A1	M2		A2	C1,M3		A3	C1,M1		A3	C1,M3	
2		M1			M1		A1	M1		A1	M1	
3		M3	C1		C1,M1,A1	C2		C1,M1	C1		C1,M1,A1	C2
4	A1			A1	C1,M1		A1	C1,M1		A1	C1,M1	
5	A1	M1,A1		A1	M1,A1		A1	A1		A1	M1,A1	
6		C2,M3,A3			C2,M2,A3	A1		C1	A1		C2,M2,A3	A1
7	A1	M2,A1		A1	C2,M2,A3	A1		C1	A1	A1	C2,M2,A3	A1
8		M1			M1			M1			M1	
9		M2		A1	C1,M2	M2	A1	C1,M2	M1	A1	C1,M2	M2
10		C2			C2			C2			C2	
11	A1	A1		A1	A1		A1	A1		A1	A1	
12		M1,A1			M1,A1		A1	M1,A1		A1	M1,A1	
13		M3	M2		M1	C1,M2		M2	C1,M1		M2	C1,M1
14	A2			A3			A3			A3		
15		C1,M3	C1		C1,M3	C1		C1,M2	C1		C1,M3	C1

16	A1	M1		A1	C1,M1		A1	C1,M1		A1	C1,M1	
17	A1	C1,M2,A3		A1	C1,A2		A1	C1,A2		A1	C1,A2	
18	A1	M2	A1	A1	C1,M2	A1		C1,M2	A1	A1	C1,M2	A1
19		C3,M1,A3	M3		C4,M1,A3	M3		C3,M1,A2	M3		C4,M1,A3	M3
20	A2	A1		A2	A1		A2	A1		A2	A1	
21		A1		A2	A1					A2	A1	
22						A1			A1			A1
23		C1,M1	M1,A1		C1,M1	M1,A1	M1	C1,M1		M1	C1,M1	M1,A1
24	A1			A1			A1			A1		
25												
26		M1		A2	C2,M1		A2	C2,M1		A2	C2,M1	
27		C1,M2			C1,M2,A1			C1,M2,A1			C1,M2,A1	
28						C1			C1			C1
29		M1			M1						M1	
30												
31		M1			C1,M1			C1			C1,M1	
total	13	60	10	20	70	13	20	49	13	24	71	17

Letter denotes anatomical position: C, cervical; M, middle; A, apical.
Arabic numeral denotes number of features identified.

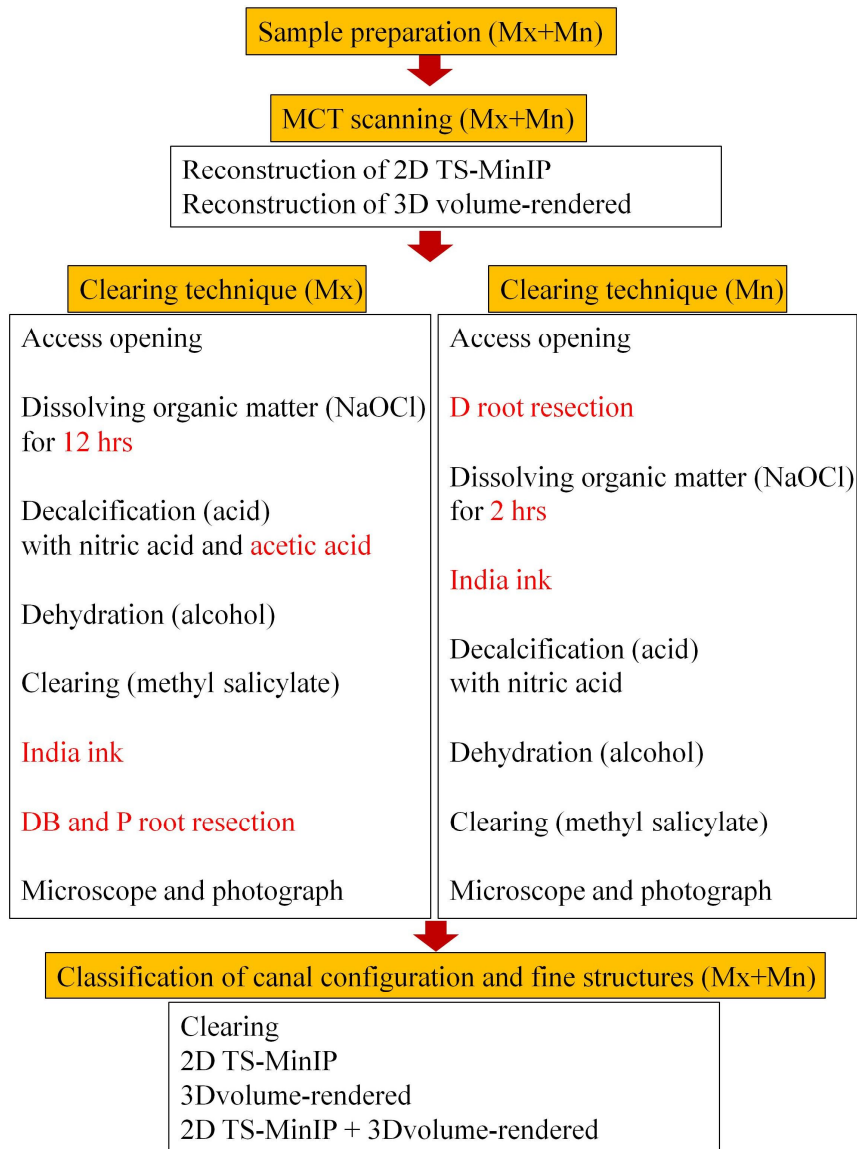


Figure 1. The flow chart of the materials and methods. The differences in the clearing technique between maxillary first molar MB roots and mandibular first molar MS roots were highlighted in red letters. (Mx: maxillary first molar, Mn: mandibular first molar, DB: distobuccal, P: palatal, D: distal)

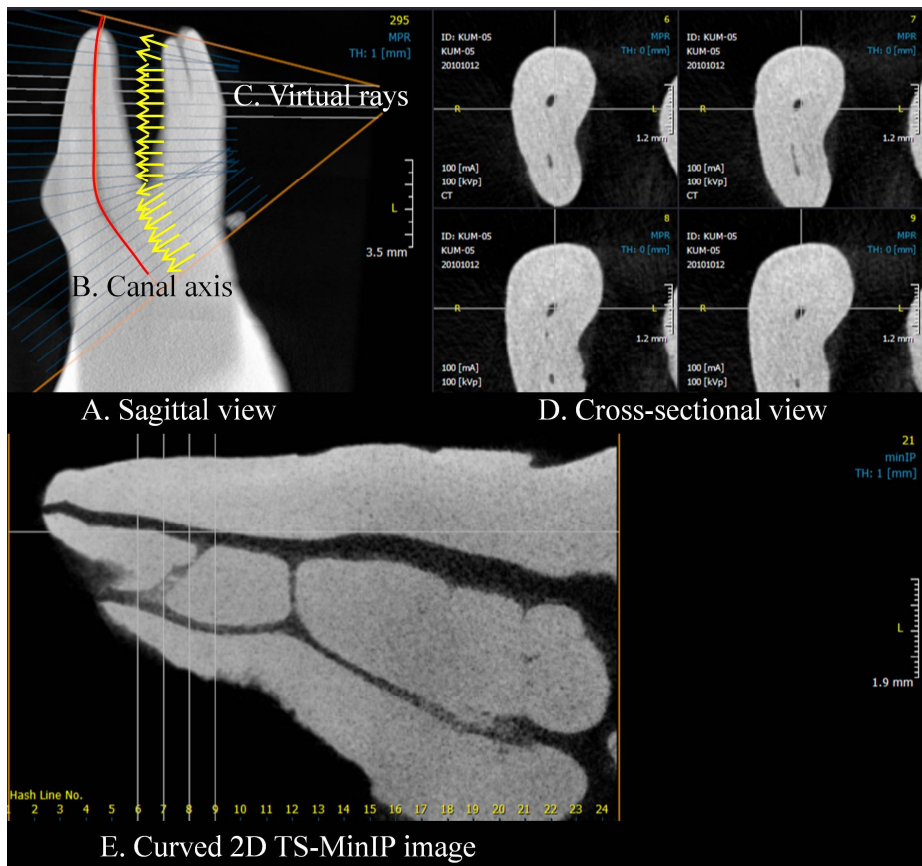


Figure 2. Schematic drawing of a curved 2D TS-MinIP technique. The volume image of the tooth was positioned with the root apex upward and it was rotated so that the more than two canals overlapped as much as possible in the sagittal view (A). The canal axis (B, red curve) was set according to the curvature of the canals. The 2D TS-MinIP image (E) recorded smallest gray value for the path of virtual rays (C, yellow arrows) passing orthogonally through the slab of canal axis (B, red curve). In cross-sectional view (D), canals having small diameters could be seen.

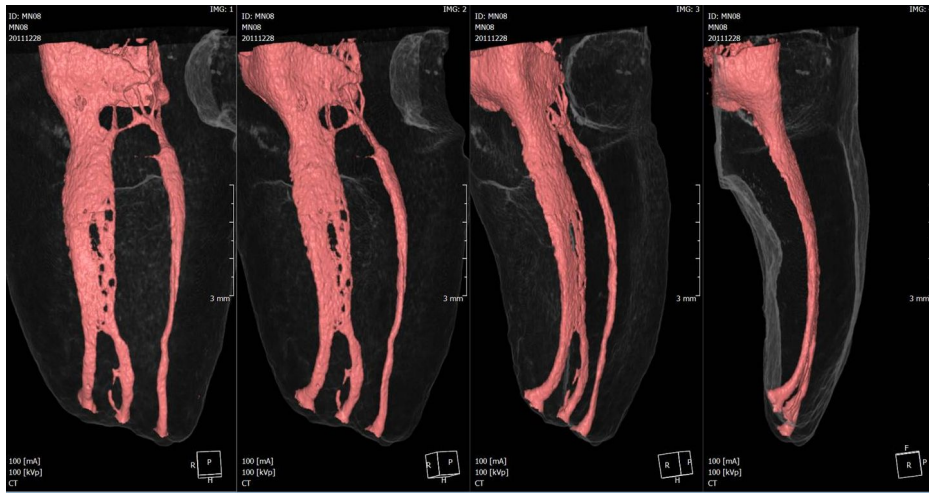


Figure 3. Representative images of the 3D volume-rendered. The canal structures were represented by an opaque red color and the external morphology of the root were rendered transparent.




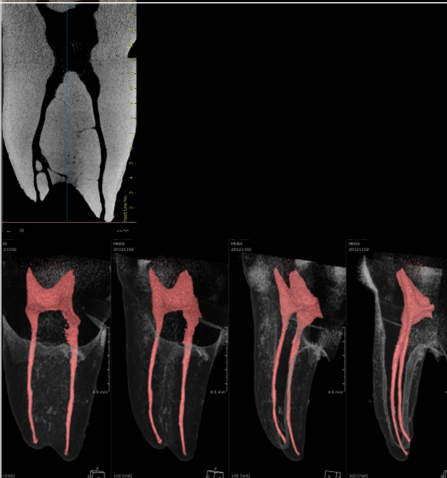
Experimental group	Representative images
Clearing	
2D TS-MinIP	
3D volume-rendered	
Combined 2D TS-MinIP and 3D volume-rendered	

Figure 4. Representative images from the clearing, the 2D TS-MinIP, the 3D volume-rendered, and the combined 2D TS-MinIP and 3D volume-rendering technique. After preparation, these 4 image sets were analyzed independently.

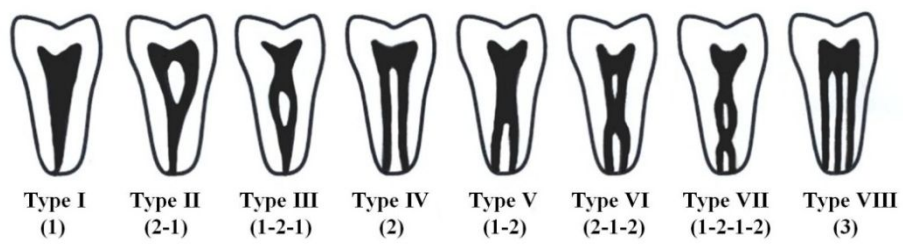


Figure 5. Representative images of 8 types of canal configuration by Vertucci (8).

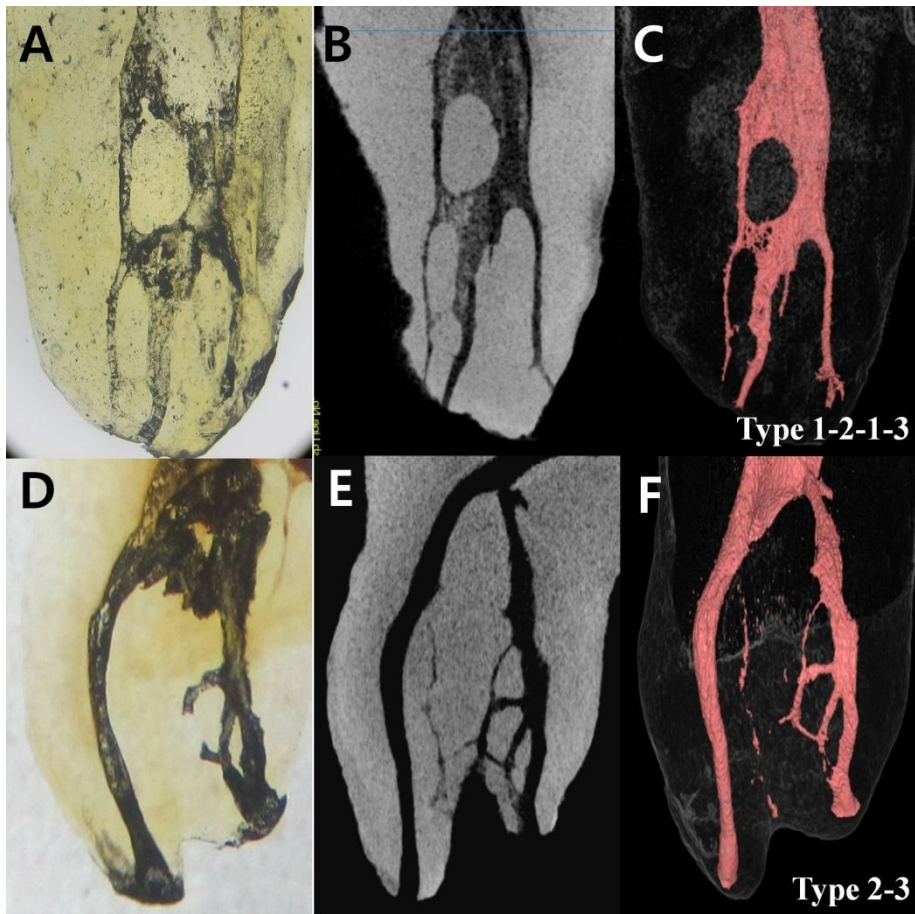


Figure 6. Representative images of some examples of non-classifiable configuration type that was not included by Vertucci classification in maxillary first molar MB roots (A, D; clearing image, B, E; 2D TS-MinIP image, C, F; 3D volume-rendered image).

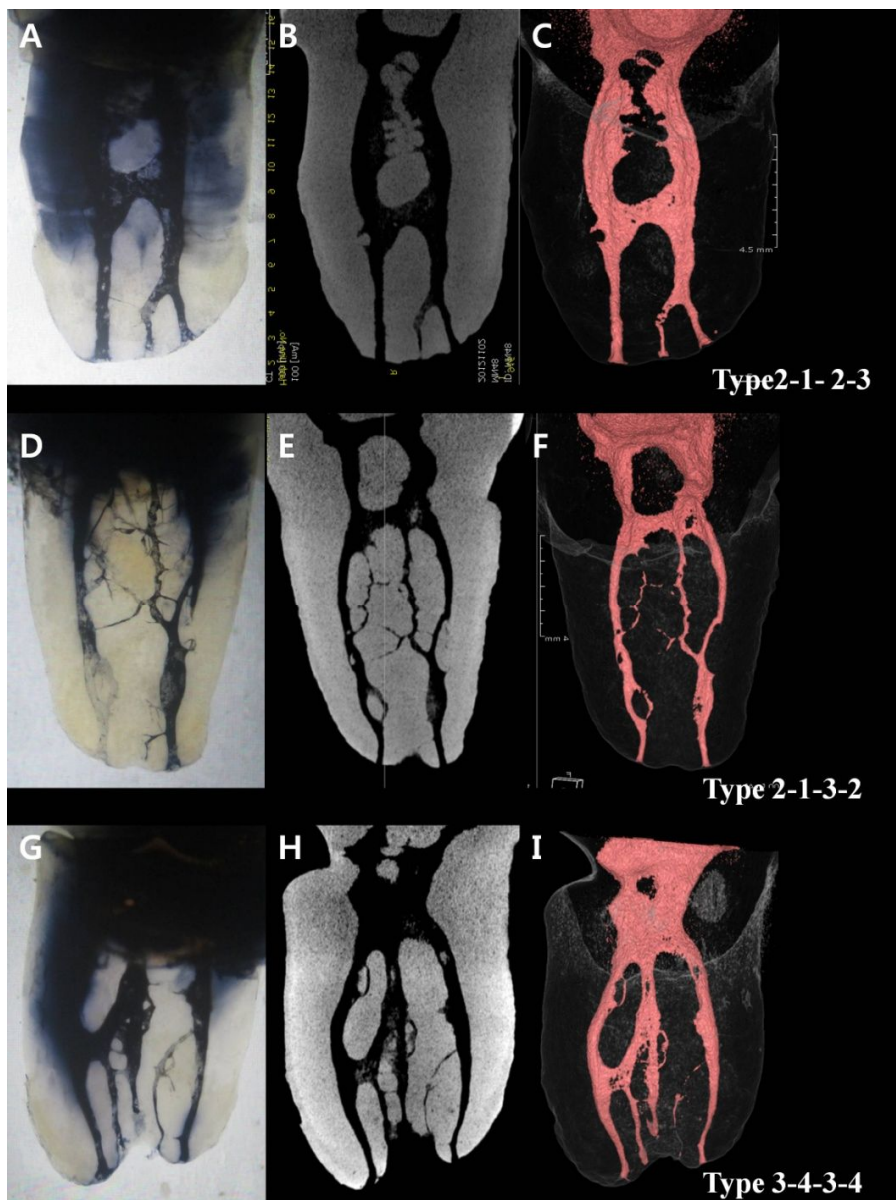


Figure 7. Representative images of some examples of new non-classifiable configuration types that were not included by Vertucci classification in mandibular first molar MS roots (A, D, G; clearing image, B, E, H; 2D TS-MinIP image, C, F, I; 3D volume-rendered image).

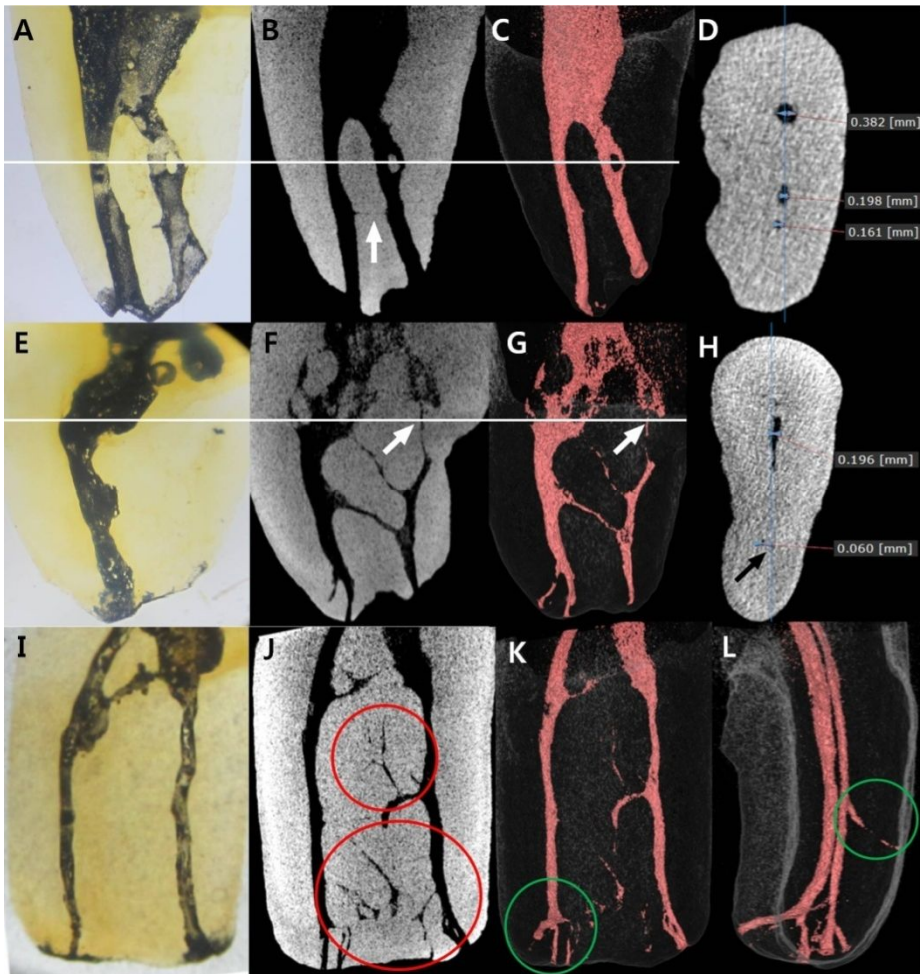


Figure 8. For 3 representative maxillary first molar MB roots, the clearing (A, E, and I), the 2D TS-MinIP (B, F, and J), and the 3D volume-rendered (C, G, K, and L) images are shown. For 2 of these roots, an MCT axial slice (D and H) at the mid-root level (horizontal white line) is also shown. In the first root, the main canals were visible in all 3 images (A–C), their large canal sizes were measured in the axial slice (D), and an intercanal communication was only visible in the 2D TS-MinIP image (B, white arrow). In the second root,

only 1 main canal was visible in the clearing image (E), a second main canal and intercanal communications were visible in the 2D TS-MinIP (F) and the 3D volume-rendered (G) images (white arrows), and the small size of the second canal that limited dye penetration was measured in the axial slice (H, black arrow). In the third root, both main canals were visible in all 4 images (I–L), fine canals were only visible in the 2D TS-MinIP image (J, red circles), and lateral canals that were hidden by the main canal were only visible in the 3D volume-rendered images (K and L, green circles).

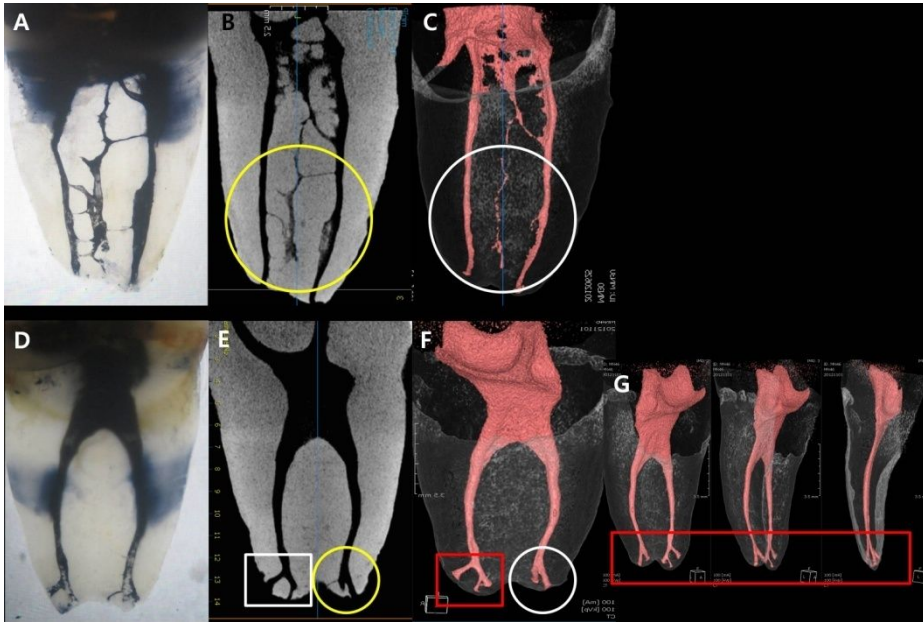


Figure 9. Comparison of three different images of a same sample of mandibular first molar MS roots (A, D; clearing image, B, E; 2D TS-MinIP image, C, F, G; 3D volume-rendered image). Generally, the 2D TS-MinIP image (B, E; yellow circles) shows more clear view of fine canal structures such as intercanal communications, accessory canals, and loops than the 3D volume-rendered image (C, F; white circles). In a clearing specimen, the ink of apical end could be washed out throughout the clearing process (D; apical area). However, a accessory canal that are perpendicular to main root canal are shown more clearly in the 3D volume-rendered images (F, G; red rectangular) than the 2D TS-MinIP image (E; white rectangular).

국문초록

상하악 제1대구치 근심협측치근과 근심치근에서의
미세전산화 단층촬영과 치아투명화 방법을 이용한
미세 근관 형태 비교

김 예 은

서울대학교 대학원 치의과학과 치과보존학 전공

(지도교수 금 기 연)

목 적

다양한 영상 재구성 기술을 이용한 미세전산화 단층촬영법은 복잡하고 미세한 근관 형태를 잘 보여준다. 본 연구는 상하악 제1대구치 근심협측치근과 근심치근의 미세 근관해부학적 근관 구조 연구를 위해, 2차원 최소강도 투시법과 3차원 볼륨-렌더링 기법으로 재구성한 미세전산화 단층촬영술 영상과 치아투명화 방법으로 얻은 영상을 비교하였다.

방 법

발거된 인간 상악 제1대구치 근심협측치근 (18개)와 하악 제1대구치 근심치근 (31개)를 미세전산화 단층촬영기 (Skyscan 1172)를 이용해 단층 영상을 획득하였다. 2차원 최소강도 투시법과 3차원 볼륨-렌더링 기법을 이용하여 미세전산화 단층촬영법 영상을 재구성하였다. 동일 치아를 투명화 처리한 후, 치아투명화 영상을 얻었다. 각 치근에서 얻은 치아투명화, 2차원 최소강도 투시, 3차원 볼륨-렌더링 영상, 그리고 2차원 최소강도 투시와 3차원 볼륨-렌더링 연합 영상을 4명의 치과의사가 독립적으로 관찰하고 Vertucci의 분류법을 토대로 근관 형태를 분류하였다. 부근관, 근관교통, 루프 등의 미세 근관 구조 역시 비교하였다.

결 과

복잡한 근관계는 치아투명화 영상보다는 미세전산화 단층촬영술 영상에서 더욱 분명하게 관찰되었다. 각 치근에서, 세 가지 미세전산화 단층촬영술 영상은 서로 같은 근관 형태를 보였던 반면, 치아투명화 영상에서는 미세전산화 단층촬영술 영상보다 덜 복잡한 형태를 보여주었다. Vertucci 분류법으로 분류되지 않은 근관 형태는 상악 제1대구치 근심치근에서는 38.9%, 하악 제1대구치 근심치근에서는 51.6%로 관찰되었다. 근관교통, 부근관, 루프와 같은 미세

근관 구조는 2차원 최소강도 투시와 3차원 볼륨-렌더링 연합 영상에서 가장 많이 발견되었다.

결 론

미세전산화 단층촬영술의 2차원 최소강도 투시와 3차원 볼륨-렌더링 연합 영상은 복잡한 근관계의 형태 연구에 유용할 것이다. 추후 본 연구에서 발견된 비분류 근관 형태를 포괄하는 근관형태 분류법의 확립은 미세 근관 형태 연구에 도움을 줄 것이다.

주요어: 근관 형태, 근관 분류, 미세전산화 단층촬영, 볼륨 렌더링, 최소 강도 투시법, 치아투명화 방법, Vertucci 분류법

학 번: 2011-31163